Electronic Supplementary Information

Tailor-Engineered Plasmonic Single-Lattices: Harnessing Localized Surface Plasmon Resonances for Visible–NIR Light-Enhanced Photocatalysis

Siew Yee Lim[1,2,3], Cheryl Suwen Law[1,2,3], Francesc Bertó-Roselló[4], Lina Liu[1,5,6], Marijana Markovic[1,7], Josep Ferré-Borrull[*4], Andrew D. Abell[*2,3,8], Nicolas H. Voelcker[*9,10,11,12], Lluís F. Marsal[*4] and Abel Santos[*1,2,3]

[1]School of Chemical Engineering and Advanced Materials, The University of Adelaide, Adelaide, South Australia 5005, Australia
[2]Institute for Photonics and Advanced Sensing, The University of Adelaide, Adelaide, South Australia 5005, Australia
[3]ARC Centre of Excellence for Nanoscale BioPhotonics, The University of Adelaide, Adelaide, South Australia 5005, Australia
[4]Department of Electronic, Electric, and Automatics Engineering, University Rovira i Virgili, Tarragona 43007, Spain
[5]State Key Laboratory of High-efficiency Utilization of Coal and Green Chemical Engineering, Ningxia University, Yinchuan 750021, P.R. China
[6]College of Chemistry and Chemical Engineering, Ningxia University, Yinchuan 750021, P. R. China
[7]School of Agriculture Food and Wine, The University of Adelaide, South Australia 5064, Australia
[8]Department of Chemistry, The University of Adelaide, South Australia 5005 Adelaide, Australia
[9]Melbourne Centre for Nanofabrication, Victorian Node of the Australian National Fabrication Facility, Monash University, Victoria 3168, Australia
[10]Monash Institute of Pharmaceutical Sciences, Monash University, Victoria 3052, Australia
[11]Commonwealth Scientific and Industrial Research Organisation (CSIRO), Victoria 3168, Australia
[12]INM-Leibniz Institute for New Materials, Campus D2 2, Saarbrücken 66123, Germany

***E-Mails:** andrew.abell@adelaide.edu.au ; nicolas.voelcker@monash.edu ; lluis.marsal@urv.cat ; abel.santos@adelaide.edu.au

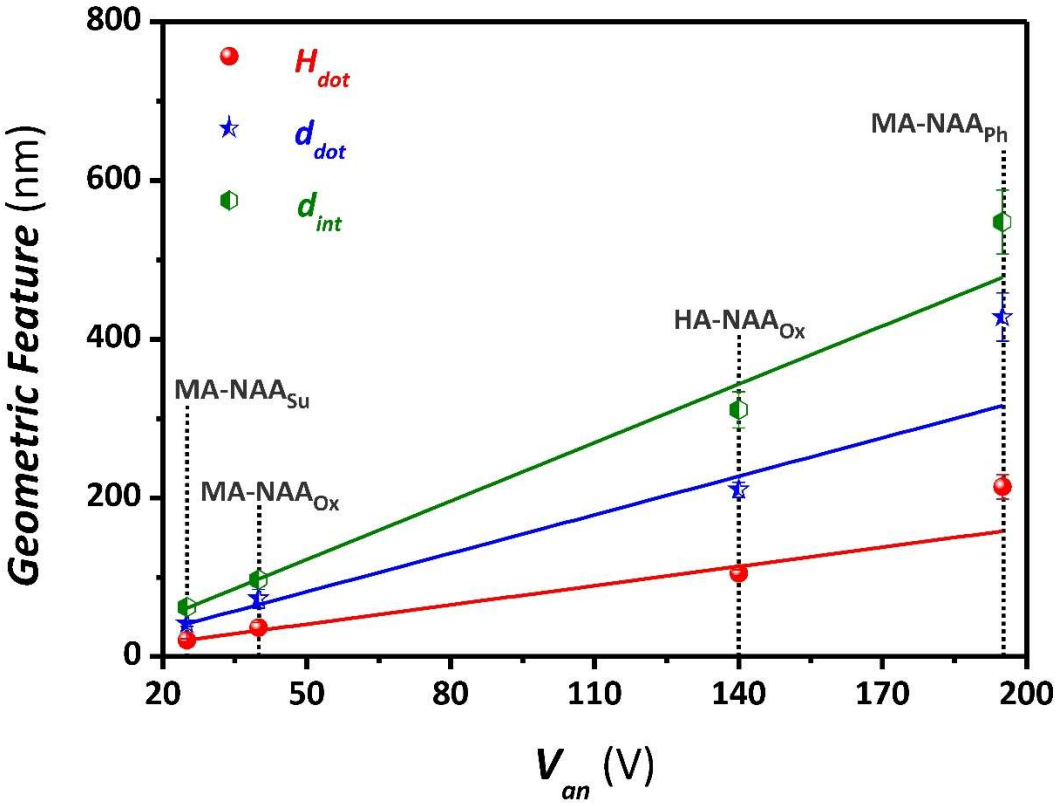

Figure S1. Linear correlation between Au-nD-PSLs geometric features (d_{int}, d_{dot} and H_{dot}) and anodization voltage (V_{an} = 25, 40, 140 and 195 V).

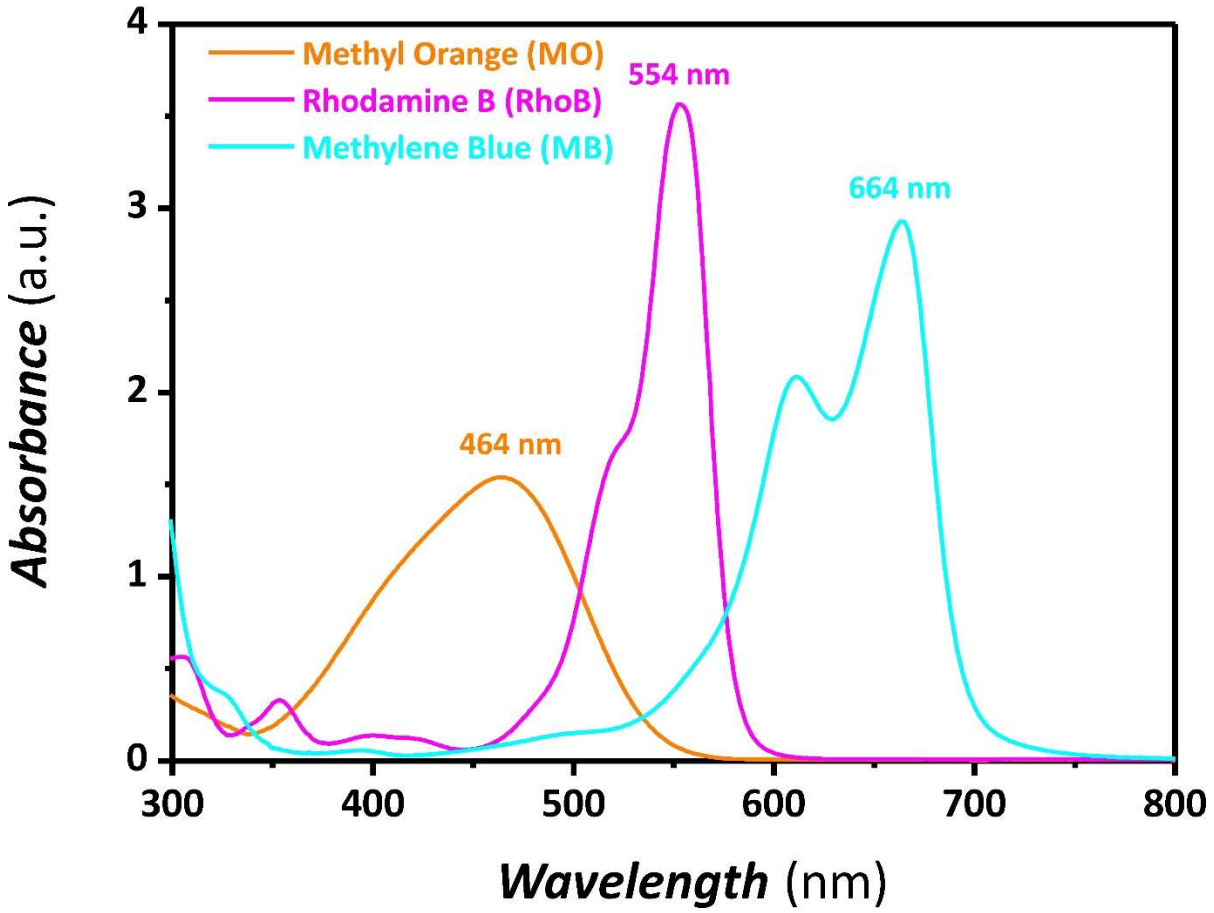

Figure S2. Absorption spectra of methylene blue (MB), rhodamine B (RhoB) and methyl orange (MO), with absorption band maxima at $\lambda_{Abs\text{-}MO}$ = 464 nm, $\lambda_{Abs\text{-}RhoB}$ = 554 nm and $\lambda_{Abs\text{-}MB}$ = 664 nm, respectively (NB: [organic] = 5 mg L^{-1}).

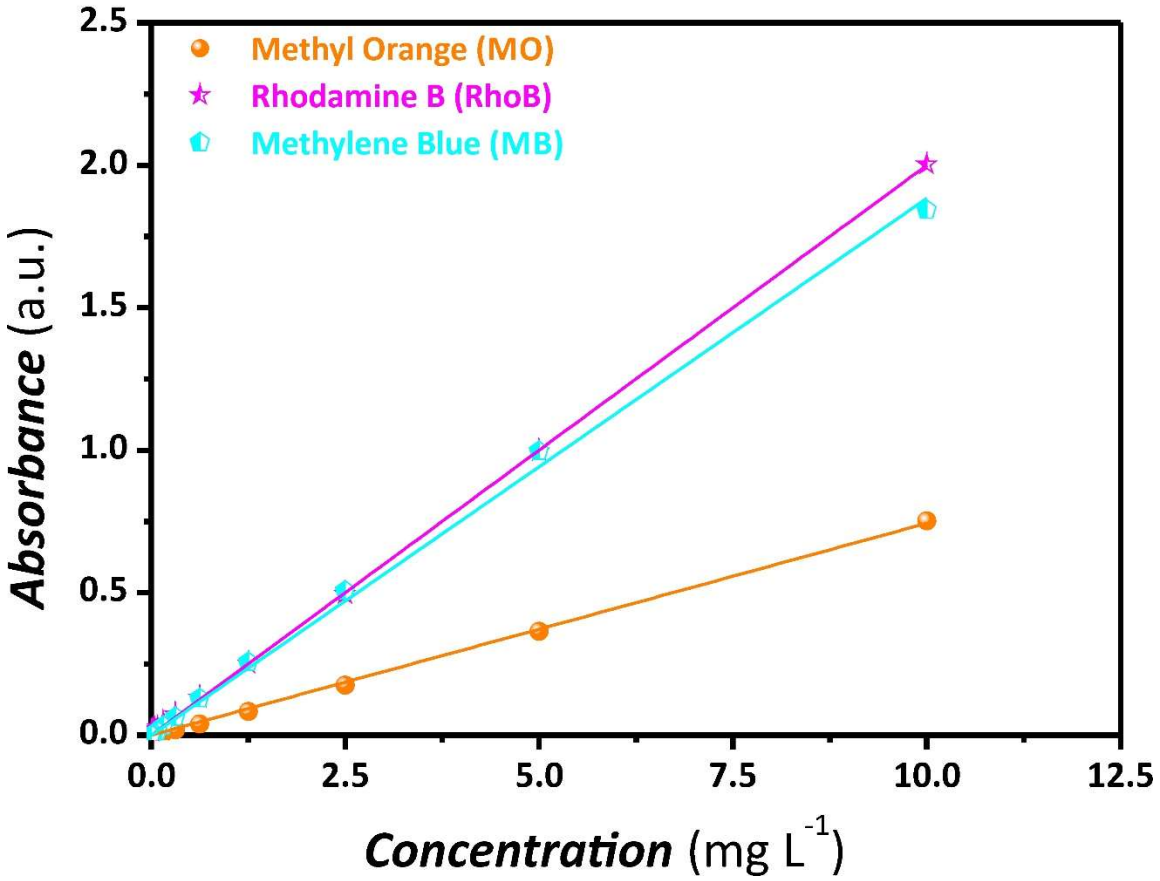

Figure S3. Linear correlation between optical absorbance and concentration of methylene blue (MB), rhodamine B (RhoB) and methyl orange (MO) (NB: concentration range from 0.00244 to 10 mg L^{-1}). The fitting lines for MB, RhoB and MO were: Abs_{MB} (a.u.) = 0.18832 *[MB]* (mg L^{-1}), Abs_{RhoB} (a.u.) = 0.19998 *[RhoB]* (mg L^{-1}) and Abs_{MO} (a.u.) = 0.07436 *[MO]* (mg L^{-1}), respectively. R^2 values for MB, RhoB and MO were 0.99852, 0.99979 and 0.99940, respectively.

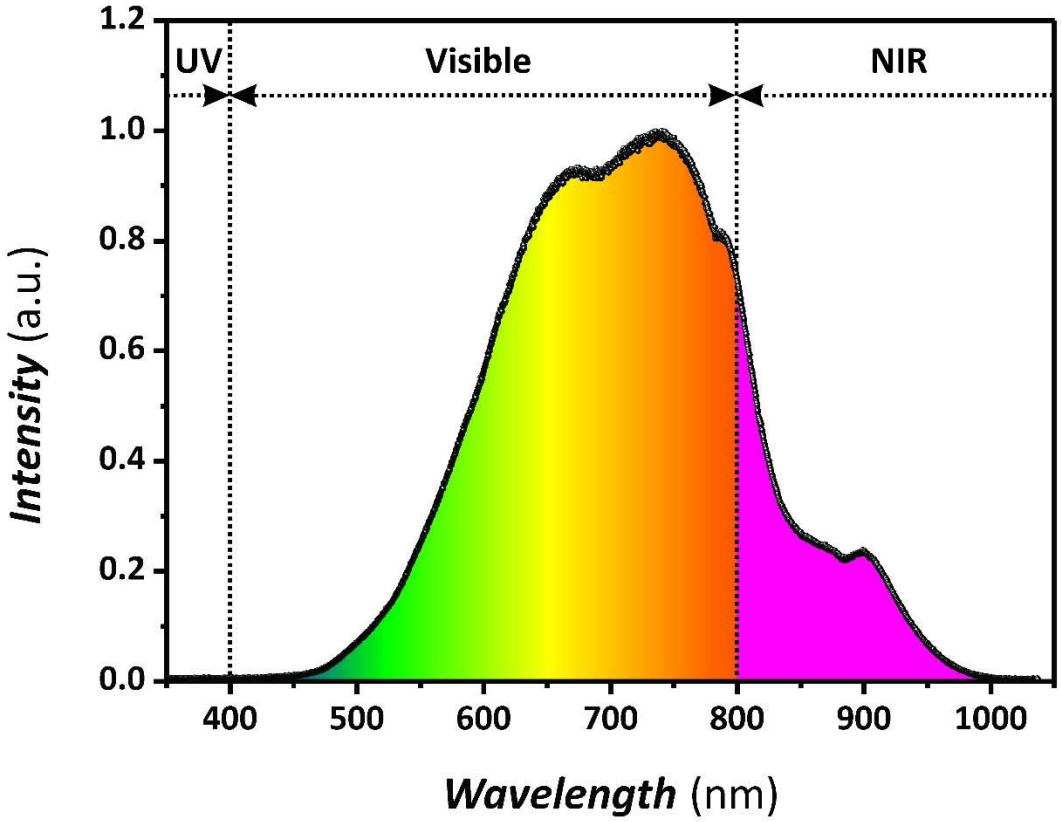

Figure S4. Irradiation spectrum of the simulated solar light irradiation source used in our study (i.e. 0.12% UV, 64.60% visible and 35.28% NIR) for the assessment of the photocatalytic degradation of model organics (NB: spectrum acquired using an optical fiber spectrophotometer USB 4000, Ocean Optics, USA).

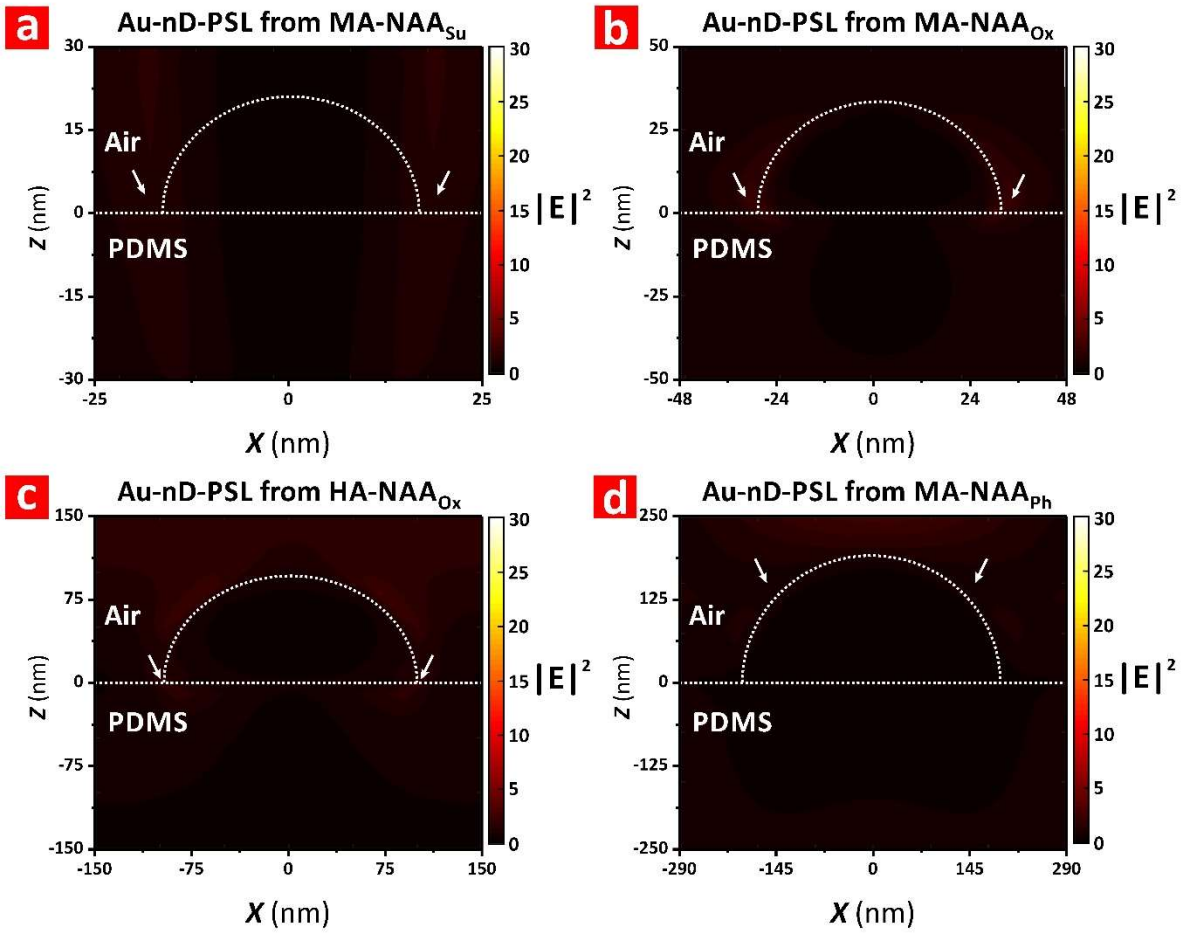

Figure S5. Cross-sectional FDTD electric field intensity ($|E^2|$) distribution profiles at non-resonant wavelengths in Au-nD-PSLs produced with: (a) MA-NAA$_{Su}$, (b) MA-NAA$_{Ox}$, (c) HA-NAA$_{Ox}$ and (d) MA-NAA$_{Ph}$ templates (NB: FDTD simulations were performed considering a PDMS substrate at the bottom of the Au nanodots and air as surrounding medium; white arrows denote sections of maximum field intensity around these plasmonic nanostructures).

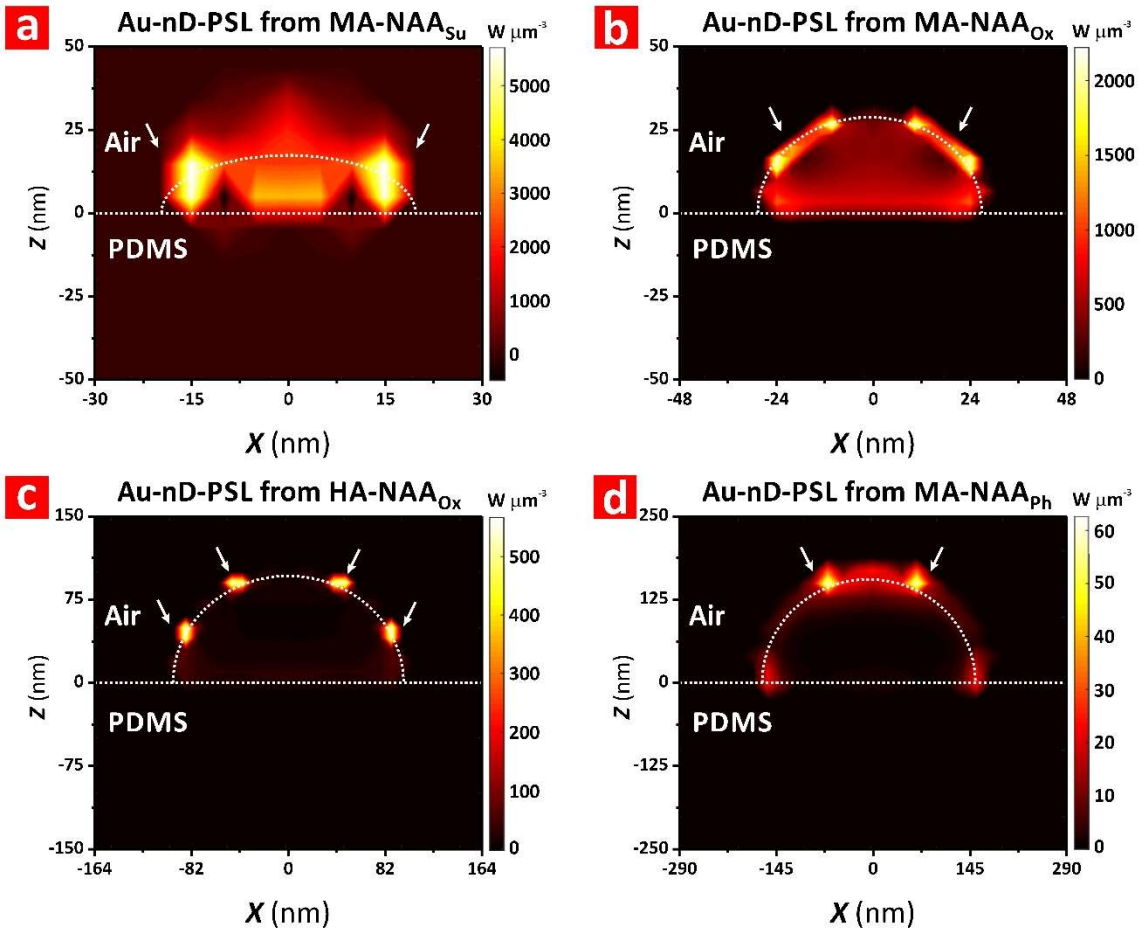

Figure S6. Cross-sectional FDTD optical absorption density distribution profiles in Au-nD-PSLs produced with: (a) MA-NAA$_{Su}$ (λ_{LSPR} = 561 nm), (b) MA-NAA$_{Ox}$ (λ_{LSPR} = 579 nm), (c) HA-NAA$_{Ox}$ (λ_{LSPR} = 627 nm) and (d) MA-NAA$_{Ph}$ (λ_{LSPR} = 618 nm) templates (NB: FDTD simulations were performed considering a PDMS substrate at the bottom of the Au nanodots and air as surrounding medium; white arrows denote sections of maximum field intensity around these plasmonic nanostructures).

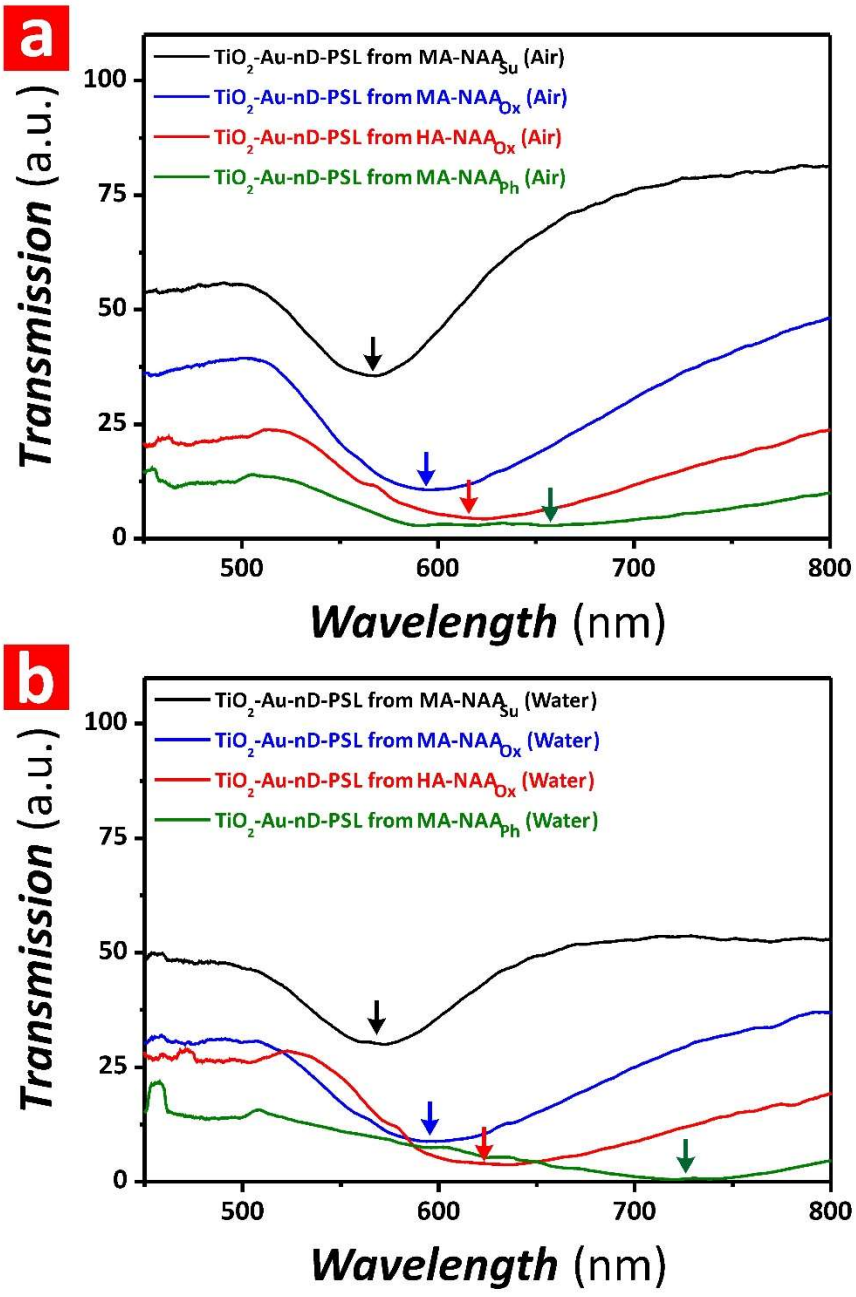

Figure S7. LSPR bands in the transmission spectra of TiO_2-Au-nD-PSLs produced with MA-NAA_{Su}, MA-NAA_{Ox}, HA-NAA_{Ox} and MA-NAA_{Ph} templates in air (a) and water (b) (NB: color arrows denote the approximate position of the central wavelength of the LSPR bands).

Lumerical Simulations

The modelling and simulations were performed by using a FDTD 3D Electromagnetic Simulator from Lumerical Inc. The optical constants of the specific material components were provided by Lumerical's material database. **Figure S8** illustrates both the computational domain and the unit cell used for the simulations. The computational domain was defined as pictured in **Figure S8a**. The dimensions were d_{int} in the X direction, $\sqrt{3}\cdot d_{int}$ in the Y direction and 106 µm in the Z direction. The plasmonic structure corresponds to a hexagonal unit cell of nanodots in an PDMS matrix, placed at the center of the computational domain reproducing the hexagonal nanodot arrangement (**Figure S8b**). An auto-nonuniform mesh was selected and automatically generated by Lumerical. Subsequently, an additional mesh refinement was incorporated in order to increase the accuracy for the simulation overriding the regions of the nanodots. The size mesh employed for these override regions was of dx = dy = dz = 3.5 nm. The plasmonic structure is periodic in X and Y directions, therefore, in order to increase computational efficiency and optimize memory requirements and computation time, periodic boundary conditions were applied in these directions. For the Z direction, in order to prevent undesirable reflections, perfectly matched layers were implemented. The optical source was an incident plane wave perpendicular to the surface of the structure (XY plane) propagating in the negative Z direction. The range of wavelengths for the optical source was from 400 to 800 nm. The reflection and transmission data were obtained by using two monitors located above and below the structure as depicted in **Figure S8a**.

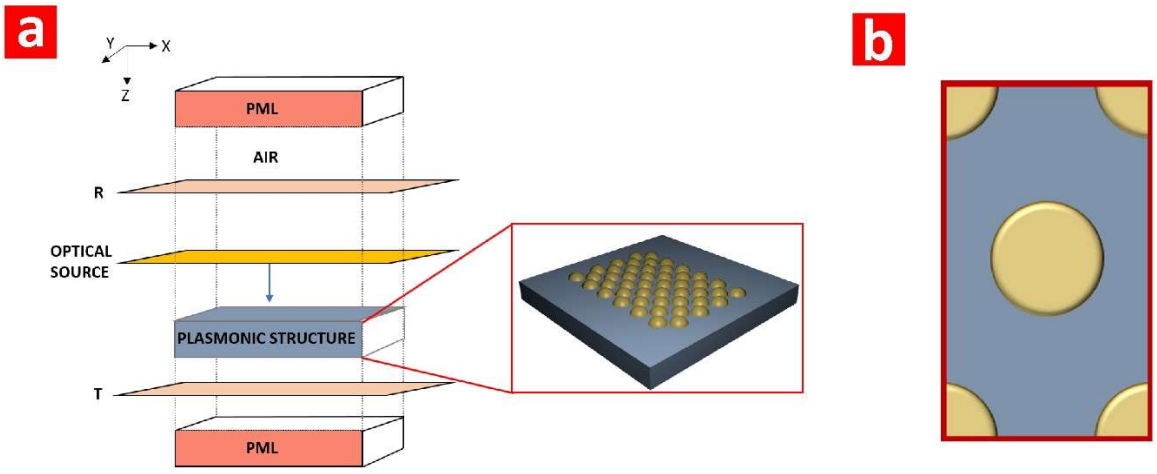

Figure S8. Illustration of the FDTD computational domain used in our study. a) Illustrative view of the computational domain where R designates the reflectance monitor, PML are perfectly matched layers, the plasmonic structure and the source re explicitly indicated. b) XY view of the FDTD unit cell: the red square designates the unit cell in the XY plane and the golden circles denote the Au nanodots.

Table S1. Anodization conditions used to produce MA-NAA_{Su}, MA-NAA_{Ox}, HA-NAA_{Ox}, and MA-NAA_{Ph} templates.

Template	***Electrolyte***	***Anodization Regime***	***Concentration*** (M)	***Temperature*** (^oC)	***Voltage*** (V)	***Time*** (h)
MA-NAA_{Su}	H_2SO_4	MA	0.3	6	25	20
MA-NAA_{Ox}	$C_2H_2O_4$	MA	0.3	6	40	20
HA-NAA_{Ox}	$C_2H_2O_4$	HA	0.3	0	140	1
MA-NAA_{Ph}	H_3PO_4	MA	0.1	–1	195	20

Table S2. Structural tunability of geometric features in Au-nD-PSLs (i.e. nanodot diameter –d_{dot}, interdot distance or lattice constant – d_{int} and nanodot height – H_{dot}) as a function of the aluminum template and the deposition time ($\tau_{D\text{-}Au}$ = 7, 15, 30 and 70 s).

Template	$\tau_{D\text{-}Au}$ (s)	d_{dot} (nm)	d_{int} (nm)	H_{dot} (nm)
MA-NAA_{Su}	7	41 ± 3	62 ± 6	21 ± 2
MA-NAA_{Ox}	15	73 ± 12	97 ± 8	36 ± 6
HA-NAA_{Ox}	30	210 ± 10	311 ± 23	105 ± 5
MA-NAA_{Ph}	70	428 ± 30	547 ± 40	214 ± 15

Table S3. Residual concentration from the photodegradation of 5 mg L^{-1} of RhoB molecules by Au-nD-PSLs produced with HA-NAA_{Ox} templates for 2 h after five photocatalytic cycles.

Photocatalytic Cycle	***Residual Concentration*** (mg L^{-1})
1	0.29 ± 0.08
2	0.36 ± 0.07
3	0.40 ± 0.07
4	0.41 ± 0.04
5	0.43 ± 0.05
Average	0.38 ± 0.06
Conversion Ratio (%)	93 ± 14

Movie S1. FDTD electric field intensity ($|E^2|$) distribution profile at resonant wavelengths in Au-nD-PSLs produced with MA-NAA_{Su} (λ_{LSPR} = 561 nm).

Movie S2. FDTD electric field intensity ($|E^2|$) distribution profile at resonant wavelengths in Au-nD-PSLs produced with MA-NAA_{Ox} (λ_{LSPR} = 579 nm).

Movie S3. FDTD electric field intensity ($|E^2|$) distribution profile at resonant wavelengths in Au-nD-PSLs produced with HA-NAA_{Ox} (λ_{LSPR} = 627 nm).

Movie S4. FDTD electric field intensity ($|E^2|$) distribution profile at resonant wavelengths in Au-nD-PSLs produced with MA-NAA_{Ph} (λ_{LSPR} = 618 nm).